Icarus **157**, 401–418 (2002)
doi:10.1006/icar.2002.6846

Galileo Photopolarimetry of Jupiter at 678.5 nm

C. J. Braak

Department of Physics and Astronomy, Free University, De Boelelaan 1081, 1081 HV Amsterdam, The Netherlands

J. F. de Haan

Department of Physics and Astronomy, Free University, De Boelelaan 1081, 1081 HV Amsterdam, The Netherlands; and Royal Netherlands Meteorological Institute, De Bilt, The Netherlands

J. W. Hovenier

Department of Physics and Astronomy, Free University, De Boelelaan 1081, 1081 HV Amsterdam, The Netherlands; and Astronomical Institute "Anton Pannekoek," Amsterdam, The Netherlands
E-mail: hovenier@nat.vu.nl

and

L. D. Travis

NASA Goddard Institute for Space Studies, 2880 Broadway, New York, New York 10025

Received October 19, 2001; revised February 7, 2002

Brightness and linear polarization measurements at 678.5 nm for four south–north strips of Jupiter are studied. These measurements were obtained in 1997 by the Galileo photopolarimeter/radiometer. The observed brightness exhibits latitudinal variations consistent with the belt/zone structure of Jupiter. The observed degree of linear polarization is small at low latitudes and increases steeply toward higher latitudes. No clear correlations were observed between the degree of linear polarization and the brightness. The observed direction of polarization changes from approximately parallel to the local scattering plane at low latitudes to perpendicular at higher latitudes. For our studies, we used atmospheric models that include a haze layer above a cloud layer. Parameterized scattering matrices were employed for the haze and cloud particles. On a pixel-wise basis, the haze optical thickness and the single-scattering albedo of the cloud particles were derived from the observed brightness and degree of linear polarization; results were accepted only if they were compatible with the observed direction of polarization. Using atmospheric parameter values obtained from Pioneer 10 and 11 photopolarimetry for the South Tropical Zone and the north component of the South Equatorial Belt, this analysis yielded acceptable results for very few pixels, particularly at small phase angles. However, for almost all pixels, acceptable results were found when the parameterized scattering matrix of the cloud particles was adjusted to produce more negative polarization for single scattering of unpolarized light, especially at large scattering angles, similar to some laboratory measurements of ammonia ice crystals. Using this adjusted model, it was found that the derived latitudinal variation of the single-scattering albedo of the cloud particles is consistent with the belt/zone structure, and that the haze optical thickness steeply increases toward higher latitudes.

Key Words: **Jupiter, atmosphere; photometry; polarimetry; radiative transfer.**

1. INTRODUCTION

The distribution and the microphysical properties of the constituents of a planetary atmosphere strongly influence the polarization of reflected sunlight and its dependence on the wavelength and phase angle. Therefore, polarimetry is a valuable tool for determining atmospheric properties of planets and satellites. Information on these properties is also important for studies of the thermal budget of planets. Polarization studies have been very successful for Venus (Hansen and Hovenier 1974, Kawabata *et al*. 1980, Sato *et al*. 1996, Knibbe *et al*. 1997, 1998, Braak *et al*. 2002). Polarimetry can be of even greater value when it is combined with brightness measurements (Mishchenko and Travis 1997a,b).

Earth-based observations of Jupiter are restricted to phase angles below 12°. Lyot (1929) was the first to conduct a thorough study of the linear polarization of Jupiter in the visible part of the spectrum. Subsequent Earth-based observations improved on his measurements in terms of wavelength range, spectral resolution, spatial resolution, and accuracy of the observations. The degree of circular polarization has also been measured but

0019-1035/02 $35.00

was found to be on the order of only 0.01% or smaller (Kemp 1974).

Studies of the phase angle dependence of linear polarization of Jupiter at visible wavelengths show that the degree of linear polarization of the central part of the jovian disk (Lyot 1929) and of the planet as a whole (Morozhenko and Yanovitskii 1973) increases from zero at 0° phase angle to several tenths of a per cent at 11° phase angle. In these cases, the reflected sunlight appears to be polarized approximately parallel to the Sun–Jupiter–Earth plane.

Studies of the distribution of linear polarization across the jovian disk (Lyot 1929, Dollfus 1957, Gehrels *et al.* 1969, Hall and Riley 1968, 1969, 1974, Carlson and Lutz 1989, Dollfus 1990) show that in comparison with the central part of the disk, the degree of linear polarization is substantially larger (at times up to 8% at visible wavelengths) at higher latitudes, while the direction of polarization there is approximately perpendicular to the nearest edge of the disk. None of these authors found significant polarization differences between belts and zones.

Interpretations of the early observations in terms of the scattering properties of atmospheric constituents were hampered by the small phase angle range. Furthermore, since efficient multiple-scattering calculations were lacking, most interpretations were only based on single-scattering considerations, which provide a first approximation (e.g., Morozhenko and Yanovitskii 1973). Also, atmospheric models often involved only very small (Rayleigh scattering) or spherical (Mie scattering) particles (e.g., Morozhenko and Yanovitskii 1973, Mishchenko 1990), while it became clear that ammonia ice crystals, which are most likely nonspherical, may be important constituents of Jupiter's upper atmosphere (Weidenschilling and Lewis 1973). In this respect, we note that Pope *et al.* (1992) reported laboratory measurements of scattering properties of ammonia ice crystals.

In the early 1970s, the adding–doubling method for multiple-scattering calculations was extended to include polarization (Hovenier 1971, Hansen 1971, Hansen and Hovenier 1971), while somewhat later, the range of phase angles at which polarization measurements of Jupiter were obtained was greatly expanded with the Pioneer 10 and 11 flybys of Jupiter, in December 1973 and December 1974, respectively. Coffeen (1974) described a north–south strip extending from $+40°$ to $-45°$ latitude at a phase angle of 103°, while Smith and Tomasko (1984) described a similar strip extending from $-45°$ to $-85°$ latitude, at a phase angle of 98°, as well as observations of the South Tropical Zone (STrZ) and the north component of the South Equatorial Belt (SEBn) at phase angles of 43, 80, 98, 103, and 120°. These studies involved measurements of the brightness and degree and direction of linear polarization in broad wavelength bands with brightness-weighted average wavelengths of 440 and 640 nm, respectively.

The north–south strip observations indicated that also at phase angles around 100°, the degree of linear polarization rises steeply with latitude, to even much higher values (up to 55%) than shown by the Earth-based observations at about the same wavelengths. Smith and Tomasko (1984) used an atmospheric model that involved a Rayleigh-scattering layer, representing scattering by molecules and small haze particles, above a Lambertian surface. They inferred that the latitudinal increase of the degree of linear polarization is caused by an increase of the optical thickness (up to about 0.5 at visible wavelengths) of the haze component of the Rayleigh-scattering layer above the main (ammonia) cloud deck. The presence of such a haze had previously been inferred from other observations (e.g., West *et al.* 1981, West *et al.* 1986) and was subsequently confirmed (e.g., Rages *et al.* 1999). The increase of the haze optical thickness with latitude is consistent with theories regarding the formation of this haze that involve bombardments of energetic particles along the magnetic field lines in the polar regions (e.g., Pryor and Hord 1991).

For the STrZ and the SEBn, Smith and Tomasko (1984) used a four-layer model, consisting (from the top down) of a gas layer, a haze layer, another gas layer, and a cloud layer. They used parameterized matrices as scattering matrices for the haze and cloud layers. For this purpose, they employed simple functions involving a small number of parameters for the elements of the scattering matrices as functions of the scattering angle. The scattering matrices that they derived for the haze particles indicate that these particles are strongly forward scattering, while producing degrees of linear polarization of up to 90% perpendicular to the scattering plane for unpolarized incident light at scattering angles of about 90°. This combination can be achieved for spherical particles only if the complex refractive index m of the particles is such that both $|m-1| \ll 1$ and $2\pi r|m-1| \ll \lambda$, where r and λ are the radius of the particle and the wavelength, respectively (Rayleigh–Gans scattering). Since such refractive indices are uncommon for compact particles suspended in a gaseous atmosphere, the haze particles are sometimes believed to be nonspherical too, or in particular, to be aggregated particles (West and Smith 1991), which is consistent with the energetic-particle bombardment hypothesis referred to above.

Smith and Tomasko (1984) concluded that the cloud particles are also strongly forward scattering but very weakly polarizing. In order to obtain the best fits, they needed the cloud particles to produce a small degree of linear polarization parallel to the scattering plane at 640 nm for single scattering at scattering angles of about 90° and for unpolarized incident light. Smith and Tomasko (1984) did not find evidence for rainbow-like features in the single-scattering behavior of the cloud particles, indicating that the cloud particles may indeed be nonspherical.

Smith and Tomasko (1984) realized that their results may not be unique: certain pairs of parameters may compensate for each other. Indeed, Smith (1986) reanalyzed polarization data from both Pioneers in combination with methane band observations (West 1979) and derived values of the degree of linear polarization of the haze particles of about 60% at a scattering angle of 90° for single scattering and unpolarized incident light, while his derived values of the haze optical thickness are higher than those derived by Smith and Tomasko (1984).

In 1996, the Galileo Orbiter was the first to measure the brightness and linear polarization of sunlight reflected by Jupiter at phase angles larger than 12° since the Pioneer 10 and 11 spacecraft. In this paper, we present a study of four south–north strips, culled from data obtained by the photopolarimeter/radiometer (PPR) on board the Galileo Orbiter, along with results obtained from model calculations. In Section 2, the instrument and the data are described. In Section 3, two nominal atmospheric models which have been used for the calculations are introduced. These models are based on those derived by Smith and Tomasko (1984), but they have been adapted to the wavelengths at which the PPR observations were made and to conform to current knowledge of constraints on scattering matrices (Hovenier and Van der Mee 1996, Braak *et al*. 2001). Results of observations are shown in Section 4 and compared with results of scattering calculations based on the nominal models. An analysis of the data in terms of spatial variability of atmospheric parameters is provided in Section 5. Section 6 is devoted to concluding remarks.

2. GALILEO PPR PHOTOPOLARIMETRY OBSERVATIONS

The photopolarimeter/radiometer (PPR) is one of the four remote-sensing instruments that are mounted on the scan platform of the Galileo Orbiter. Of its main objectives, the most relevant for this work is to determine the vertical and horizontal distribution of cloud and haze particles in the atmosphere of Jupiter, including their size, shape, and refractive index (Russell *et al*. 1992).

For each of the PPR's three functions—photometry, photopolarimetry, and radiometry—the radiation from a scene is collected by a telescope and focused onto a circular field stop subtending 2.5 mrad. At a planetocentric distance of 700,000 km, which is typical for the observations studied in this paper, the footprint at the center of the disk has a diameter of 1750 km. Radiation that passed the field stop is modified by passage through optical elements located on one of the 32 positions of a filter wheel. While the telescope footprint on the target body (Jupiter or any of its satellites) moves, the filter wheel steps either through all positions, or through a subset of these positions (depending on the objective of the observation). This stepping can be done in one single direction or in alternating directions. In that manner, areas of the target body are scanned quasi-simultaneously using different filters. The filter wheel steps sufficiently fast with respect to the movement of the footprint across the disk so that measurements of about a dozen successive scenes may be combined into properties such as brightness and the state of polarization of one so-called *pixel*, as if the individual scenes overlap exactly.

For photopolarimetry, nine filter positions are used, three for each of the three photopolarimetry wavelengths, 410.0, 678.5, and 944.6 nm (see Table I). The bandwidths given in Table I are sufficiently narrow so that measurements for those bands may be treated as monochromatic at the center wavelength. For each wavelength, the three filter positions contain, apart from the appropriate bandpass filter, halfwave retarders, each rotated 22.5° from one filter position to the next. After passing the filter wheel, the light is directed through a Wollaston prism that serves as a polarizing beam-splitter and produces two spatially separated and orthogonally polarized output beams, the intensities of which are measured by two silicon photodiodes. Thus, six measurements are potentially available per wavelength for computing the properties of the reflected light for a pixel. For a perfect instrument measuring a scene with constant reflection properties, two of these six measurements are redundant since the first and third positions listed for each wavelength in Table I yield essentially the same results, but with the beams produced by the Wollaston prism interchanged. When employing all three filter positions for a wavelength during an observation, this apparent redundancy was used to determine the brightness and state of polarization of the reflected light with higher accuracy, by monitoring the relative responsivities of the two silicon photodiodes.

TABLE I
Galileo PPR Polarimetry Filters

Center wavelength (nm)	Full width at half maximum (nm)	Filter positions
944.6	10.8	1, 3, 5
678.5	8.7	7, 9, 11
410.0	60.0	13, 15, 17

The observed brightness and state of polarization that we used are archived at the Planetary Data System in the form of the brightness $I_{\rm obs}$ in W cm^{-2} sr^{-1} nm^{-1}, the degree of linear polarization $P_{\rm obs}$, and the direction of polarization $\tilde{\chi}_{\rm obs}$ in degrees. The tilde in $\tilde{\chi}_{\rm obs}$ indicates that this quantity is measured relative to the reference plane of the instrument, namely the instrument baseplate, which maintained a stable orientation in space.

For the observations and for results of multiple-scattering calculations, the degree of linear polarization P is defined in terms of Stokes parameters as

$$P = \frac{\sqrt{Q^2 + U^2}}{I}. \tag{1}$$

As P is always nonnegative, we do not speak of "negative" or "positive" polarization for the observations and for results of multiple-scattering calculations, but depending on the corresponding direction of polarization χ, we use the expressions "polarized approximately parallel" or "approximately perpendicularly" to the pertinent reference plane (e.g., the local scattering plane or the instrument baseplate). Alternatively, for cases in which $U = 0$, we define the *signed* degree of linear polarization $P_{\rm s}$ as

$$P_{\rm s} = -\frac{Q}{I}. \tag{2}$$

This is especially true for single scattering if the incident light is unpolarized. P_s is negative if the light is polarized parallel to the reference plane, and it is positive if the light is polarized perpendicularly to that plane. Thus, for light scattered once, we use the terms "negative polarization" and "positive polarization" accordingly if the incident light is unpolarized.

As determining the degree of linear polarization was considered to be the most important goal for the photopolarimetric measurements, no reliable inflight calibration of the photodiodes has been performed, and the preflight accuracy may have been on the order of 10%. This is of no consequence to the accuracy of P_{obs} and $\tilde{\chi}_{obs}$, since these quantities are defined in terms of intensity ratios, but may result in systematic errors of I_{obs}. Even though the systematic errors in the brightness may be large, its random errors due to noise, ΔI_{obs}, which are estimated to be no larger than 0.001 μW cm^{-2} sr^{-1} nm^{-1}, can generally be ignored. As mentioned above, the greatest effort was put into obtaining P_{obs}. Its accuracy, ΔP_{obs}, is estimated to be the larger of $(0.06 \times P_{obs})$ and 0.003. Errors in $\tilde{\chi}_{obs}$ are not known.

In our analyses, we prefer to use directions of polarization χ (without tilde) referenced to the local scattering plane (i.e., the plane defined by the Sun-pixel and pixel-detector directions). Further, we measure χ counter-clockwise when looking in the direction of propagation and choose its value, $0^\circ \le \chi < 180^\circ$, so that $\cos 2\chi$ has the same sign as Stokes parameter Q (Hovenier and Van der Mee 1983). However, the instrument baseplate is used as the reference plane for the observations, and neither the orientation of this plane with respect to the local scattering plane nor the sense in which $\tilde{\chi}_{obs}$ is measured (clockwise or counterclockwise when looking in the direction of propagation) are fully documented. Therefore, we can write down the following relation between $\tilde{\chi}_{obs}$ and the observed direction of polarization with respect to the local scattering plane, χ_{obs}:

$$\chi_{obs} = \chi_0 \pm \tilde{\chi}_{obs}. \quad (3)$$

For obtaining the value of χ_0, we use the fact that the sunlight reflected by Jupiter's high latitude regions is polarized approximately perpendicularly to the local scattering plane, i.e., $\chi_{obs} \approx 90^\circ$ (e.g., Coffeen 1974). Now in the data pertaining to the four south–north strips under consideration here, $\tilde{\chi}_{obs}$ is close to 0° in those regions. This means that the baseplate is oriented approximately perpendicularly to the local scattering plane and thus that $\chi_0 = 90^\circ$ is a good approximation. Since the values of $\tilde{\chi}_{obs}$ range from -90 to 90° in the dataset, this value for χ_0 also ensures that the corresponding values of χ_{obs} fall within the range $0^\circ \le \chi_{obs} < 180^\circ$, regardless of the choice of the sign in Eq. (3).

The properties of the reflected sunlight for a pixel are supplemented in the dataset with the pixel's planetocentric latitude, the angle between the pixel-detector and pixel-zenith directions, θ, the angle between the pixel-Sun and the pixel-zenith directions, θ_0, and the local phase angle α (the angle between the pixel-Sun and pixel-detector directions).

In this paper, we focus on photopolarimetric data from four south–north strips that have been observed in May and June 1997 (see Table II and Fig. 1). These strips are the only ones obtained during Galileo's nominal mission that cover large latitude ranges. We consider only the 678.5-nm observations, as that is the only wavelength for which observations were performed during both orbits, and because it is relatively close to 640 nm, which is the wavelength at which the Pioneer 10 and 11 Imaging Photopolarimeter (IPP) instruments performed similar observations. To avoid cluttering in the figures in the remainder of this paper, a selection was made from the available pixels such that the selected pixels were spaced by about 1.25 mrad (one-half of the field-stop diameter) as seen from the orbiter. This selection has no influence on our conclusions.

3. OPTICAL MODEL OF THE ATMOSPHERE

The light scattered by Jupiter is not caused only by single scattering of the sunlight but also by multiple scattering by the molecules and particles in the atmosphere. We employ the adding–doubling method (Hansen 1971, Hovenier 1971, De Haan *et al.* 1987), which takes all orders of scattering into account, for obtaining the reflection properties for models of Jupiter's atmosphere. In order to compute values for the brightness of the reflected light from calculated reflection properties, we need to know the flux of the incident sunlight, πF. This flux was calculated for the G8 and C9 orbits separately, using orbital elements from the *Astronomical Almanac* of 1997 (U.S. Government Printing Office 1997) and fluxes at 1 astronomical unit from tables of Neckel and Labs (1984). The resulting values

TABLE II
Summary of the Galileo PPR Observations of Jupiter Used in This Study

Strip number	Orbit	Data filename	Date	Min./max. local phase angle (°)	Median planetocentric distance (km)	Observed wavelengths (nm)
1	G8	NSSTRP01	8 May 1997	13.1/15.1	717,900	678.5, 944.6
2	G8	NSSTRP02	8 May 1997	49.8/51.3	704,700	678.5, 944.6
3	C9	NSSTRP02	27 Jun 1997	49.0/50.9	866,500	410.0, 678.5
4	C9	NSSTRP03	28 Jun 1997	98.1/98.9	1,418,000	410.0, 678.5

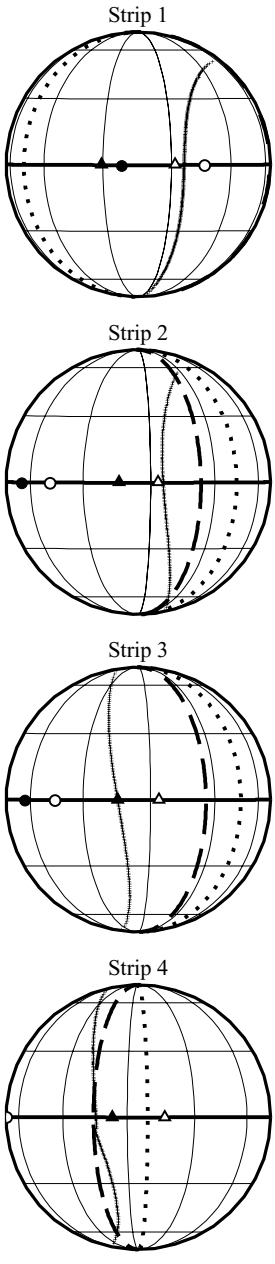

FIG. 1. Projected globes of Jupiter showing the four south–north strips considered in this paper (solid thick curves). Each strip was scanned from south to north (north is at the top). Dotted and dashed thick curves: terminators at the start and stop times of the strip observations, respectively. Open and filled triangles: subspacecraft points at those times, respectively. Open and filled circles: subsolar points at those times, respectively.

are $\pi F = 5.80\ \mu\text{W cm}^{-2}\ \text{nm}^{-1}$ (G8) and $5.83\ \mu\text{W cm}^{-2}\ \text{nm}^{-1}$ (C9).

The atmospheric model consists of a number of plane-parallel layers, each of which is characterized by an optical thickness b, a single-scattering albedo a, and a scattering matrix $\mathbf{F}$. If we assume that the particles in the layers are randomly oriented and occur in equal numbers as their mirror particles, the scattering matrix at a certain wavelength consists of at most six independent nonzero elements that are only functions of the scattering angle and the size, shape, and composition of the particles (see Van de Hulst 1957). If the scattering plane acts as the reference plane, the scattering matrix can be written as

$$\mathbf{F}(\Theta) = \begin{bmatrix} F_{11}(\Theta) & F_{21}(\Theta) & 0 & 0 \\ F_{21}(\Theta) & F_{22}(\Theta) & 0 & 0 \\ 0 & 0 & F_{33}(\Theta) & F_{34}(\Theta) \\ 0 & 0 & -F_{34}(\Theta) & F_{44}(\Theta) \end{bmatrix}, \quad (4)$$

where Θ is the scattering angle (the angle between the directions of the incident and scattered beams). $F_{11}(\Theta)$ is often called the *phase function* and $F_{21}(\Theta)$ is related to the signed degree of linear polarization P_s of the reflected light for unpolarized incident light by

$$P_s(\Theta) = -\frac{F_{21}(\Theta)}{F_{11}(\Theta)}. \quad (5)$$

In this paper, we normalize all scattering matrices so that the average of $F_{11}(\Theta)$ over all directions is unity, i.e.,

$$\frac{1}{2}\int_{-1}^{1} F_{11}(\Theta)\mathrm{d}\cos\Theta = 1. \quad (6)$$

The atmospheric models treated in this paper are based on those used by Smith and Tomasko (1984) for their analysis of Pioneer 10 and 11 photopolarimetry. These models consist of four atmospheric layers, namely, from the top down, (1) a pure gas layer, (2) a haze layer, which consists of gas and haze particles, (3) another pure gas layer, and (4) a semiinfinite cloud layer, which consists of gas and cloud particles (see Fig. 2).

Since the shapes of the haze and cloud particles are unknown, other than that they are probably nonspherical, the single-scattering characteristics of the haze and cloud layers are given by so-called *parameterized scattering matrices* (Braak *et al.* 2001), using the following simple functions for elements or

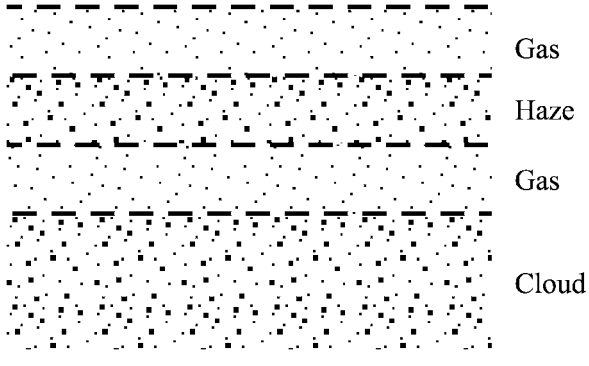

FIG. 2. Schematic representation of the atmospheric model.

element ratios of the scattering matrix.

$$F_{11}(\Theta) = P_{\mathrm{HG}}(g, \Theta) \tag{7}$$

or

$$F_{11}(\Theta) = f_1 P_{\mathrm{HG}}(g_1, \Theta) + (1 - f_1) P_{\mathrm{HG}}(g_2, \Theta), \tag{8}$$

$$-\frac{F_{21}(\Theta)}{F_{11}(\Theta)} = p \frac{\sin^2 \Theta}{1 + \cos^2 \Theta}, \tag{9}$$

$$\frac{F_{22}(\Theta)}{F_{11}(\Theta)} \equiv 1, \tag{10}$$

$$\frac{F_{33}(\Theta)}{F_{11}(\Theta)} = \frac{2 \cos \Theta}{1 + \cos^2 \Theta}, \tag{11}$$

$$F_{34}(\Theta) \equiv 0, \quad \text{and} \tag{12}$$

$$F_{44}(\Theta) \text{ is not specified,} \tag{13}$$

where $-1 < g < 1$ is called the asymmetry parameter, $0 \leq f_1 \leq 1$ is a weight factor, and $-1 \leq p \leq 1$ is called the polarization parameter. P_{HG} is defined as

$$P_{\mathrm{HG}}(g, \Theta) = \frac{1 - g^2}{(1 + g^2 - 2g \cos \Theta)^{3/2}}. \tag{14}$$

Since this function was introduced by Henyey and Greenstein (1941), the functions in Eqs. (7) and (8) are often called one-term and two-term Henyey–Greenstein functions, respectively. If $p = 1$, Eqs. (9)–(12) hold exactly for Rayleigh scattering without depolarization. Since Stokes parameter V has not been measured by the PPR, and since it is decoupled from the other Stokes parameters (because of Eq. (12)), there is no need to specify $F_{44}(\Theta)$. However, it can be shown that for any set of parameter values, a function $F_{44}(\Theta)$ exists so that Eqs. (7)–(13) provide parameterized scattering matrices which obey all constraints that are known for scattering matrices (Hovenier and Van der Mee 1996, Braak *et al.* 2001). Previously, Smith and Tomasko (1984), among others, assumed that

$$F_{33}(\Theta) = F_{11}(\Theta). \tag{15}$$

This choice is sometimes motivated by noting that, for spheres, $F_{33}(\Theta)$ resembles $F_{11}(\Theta)$ for a large part of the scattering angle range (Tomasko and Smith 1982, Tomasko and Doose 1984). However, employing Eq. (15) instead of Eq. (11) would yield a matrix that does not obey all constraints (Hovenier and Van der Mee 1996, Braak *et al.* 2001) and may therefore give unphysical results, unless $p = 0$. We note that the results of our model calculations depend only marginally on the choice between these two parameterizations of $F_{33}(\Theta)$.

We chose parameter values for two nominal models that are based on results of Smith and Tomasko (1984) for the South Tropical Zone (STrZ) and the north component of the South Equatorial Belt (SEBn) at 640 nm, respectively. These two models differ only in the single-scattering albedo of the cloud particles. The model parameters and their values are summarized in Table III.

TABLE III
Properties of the Nominal Models

Property	Symbol	Value
Gas layer 1		
Optical thickness	b_{g1}	0.0067
Single-scattering albedo	a_{g1}	1.0
Depolarization factor	δ_{g1}	0.0
Haze layer		
Optical thickness	b_{h}	0.0625
Single-scattering albedo	a_{h}	0.95
Parameterized scattering matrix	g_{h}	0.75
	p_{h}	0.9
Gas layer 2		
Optical thickness	b_{g2}	0.011
Single-scattering albedo	a_{g2}	1.0
Depolarization factor	δ_{g2}	0.0
Cloud layer		
Optical thickness	b_{c}	∞
Single-scattering albedo	a_{c}	0.997 (StrZ)
		0.9925 (SEBn)
Parameterized scattering matrix	$g_{1,\mathrm{c}}$	0.80
	$g_{2,\mathrm{c}}$	−0.70
	$f_{1,\mathrm{c}}$	0.938
	p_{c}	−0.05

In order to obtain optical thicknesses of the gas layers at 678.5 nm from those given by Smith and Tomasko (1984) at 640 nm, we applied the Rayleigh law that molecular optical thicknesses are proportional to λ^{-4}. Further, we used the Rayleigh scattering matrix (Chandrasekhar 1950) with a depolarization factor $\delta = 0$ for both gas layers, since we are dealing with a hydrogen/helium atmosphere. We assumed the albedo of single scattering of the gas layers to be equal to unity.

At the wavelength of the observations under consideration, the contribution by molecules to the total light scattered by the cloud and haze layers is negligible. Since for the haze and cloud particles, the wavelength dependencies of the scattering matrices, the scattering cross sections, and the single-scattering albedos are not known, no effort has been made to convert the corresponding parameter values of Smith and Tomasko (1984) at 640 nm to values at 678.5 nm. We expect that this small wavelength difference does not affect our conclusions. As the polarization of reflected sunlight is mainly influenced by atmospheric constituents up to an optical depth of only approximately 2, the scattering matrix of the cloud layer in the model can be assumed to be mostly representative for the upper part of the ammonia cloud layer.

For later reference, Fig. 3 shows the functions $F_{11}(\Theta)$ and $-F_{21}(\Theta)/F_{11}(\Theta)$ of the scattering matrices of the gas, haze, and cloud particles of the nominal models.

In order to perform multiple-scattering calculations, the relative azimuth, $\phi - \phi_0$, between the Sun-pixel and pixel-detector

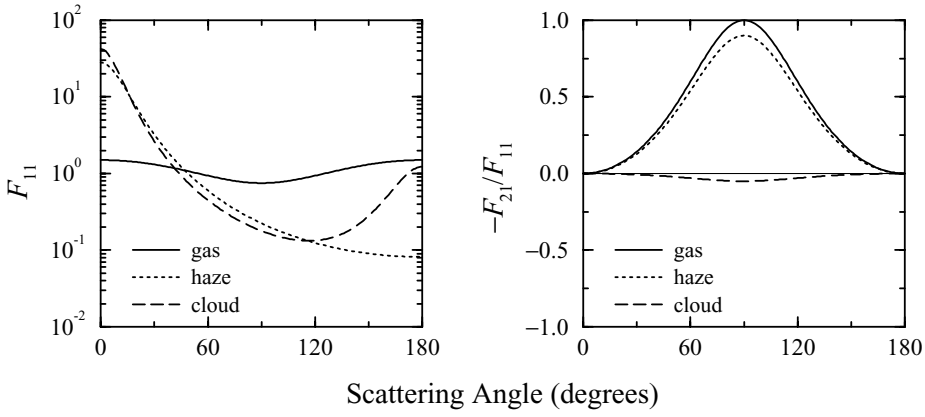

FIG. 3. The functions $F_{11}(\Theta)$ and $-F_{21}(\Theta)/F_{11}(\Theta)$ of the scattering matrices of the gas, haze, and cloud particles in the nominal models.

directions is computed from the angles θ, θ_0, and α (see Section 2) by using

$$\cos(\phi - \phi_0) = \frac{\mu\mu_0 - \cos\alpha}{(1-\mu^2)^{1/2}\left(1-\mu_0^2\right)^{1/2}} \qquad (16)$$

(Horak 1950), where $\mu = \cos\theta$ and $\mu_0 = \cos\theta_0$. If the pixel is located north of the intensity equator, and the subsolar point is located east of the suborbiter point, the value of $\phi - \phi_0$ must obey $0^\circ \le \phi - \phi_0 \le 180^\circ$. From symmetry relations (Hovenier 1970), the same interval applies if the pixel is located south of the intensity equator and the subsolar point is located west of the suborbiter point, whereas $180^\circ \le \phi - \phi_0 \le 360^\circ$ must be taken otherwise.

The fact that the adding–doubling method requires the layers in the atmosphere model to be plane-parallel makes this method unsuitable for pixels with nearly grazing angles θ or θ_0. Therefore, only pixels with both $\mu > 0.15$ and $\mu_0 > 0.15$ are considered for the calculations reported in this paper. Results in Section 19.2.2 of Van de Hulst (1980) indicate that the plane-parallel approximation yields progressively more erroneous results for μ and μ_0 smaller than this value.

4. QUALITATIVE INTERPRETATION OF THE OBSERVATIONS

In Fig. 4, observed values of the brightness, degree of linear polarization, and direction of polarization are compared with results of calculations for the nominal models. Belt/zone boundaries are indicated as an aid in interpreting small-scale structures. Here, the plus sign in Eq. (3) is used for computing the observed direction of polarization with respect to the local scattering plane. As explained in the preceding section, only pixels with $\mu > 0.15$ and $\mu_0 > 0.15$ were considered for the calculations. This prevents the calculated curves in Fig. 4 from extending as far toward the poles as the observed values.

We identify the following striking features. The observed brightness shows substantial structure, much of which correlates with the zone/belt divisions of the jovian atmosphere as expected: the belts are darker than the zones. This is especially the case near the equator. Previously, Smith and Tomasko (1984) ascribed the differences in reflectivity between the belt and zone they studied to differences in the single-scattering albedo of the cloud particles. It seems plausible that this is the case here as well (see Section 5), since varying the single-scattering albedos of any of the other layers will not affect the calculated brightness very much because (i) the haze and gas layers are relatively optically thin and (ii) the angles θ and θ_0 in the south–north strips under study are generally not near grazing for equatorial and midlatitude regions. As mentioned above, random errors ΔI do not exceed 0.001 μW cm^{-2} sr^{-1} nm^{-1} and are thus negligible (see Fig. 4).

The observed degree of linear polarization increases dramatically towards both poles. Part of this increase can be explained by the fact that at higher latitudes, the contribution to the observed polarization by the upper layers of the atmosphere is enhanced owing to the higher values of θ and θ_0 at those latitudes. Since these upper layers are more strongly polarizing than the underlying cloud layers (cf. Fig. 3), the observed degree of linear polarization is higher at high latitudes than it is near the equator. However, as the results of the calculations in Fig. 4 show, this increase of the degree of linear polarization is not sufficient to explain the observations, or in other words, it is only part of the observed increase, as Smith and Tomasko (1984) already pointed out. We also performed computations for a number of other atmosphere models, but we could not find any horizontally homogeneous model that could satisfactorily fit the polarization observations at all latitudes. This is consistent with other types of observations that suggest that the jovian stratospheric haze (which may be identified with the haze layer in our model) is more prominent in polar regions than near the equator (e.g., West *et al.* 1981, Rages *et al.* 1999). An increase of the haze optical thickness towards higher latitudes is consistent with the observations shown in Fig. 4, since such an increase would increase the calculated degree of linear polarization at high latitudes (see Section 5).

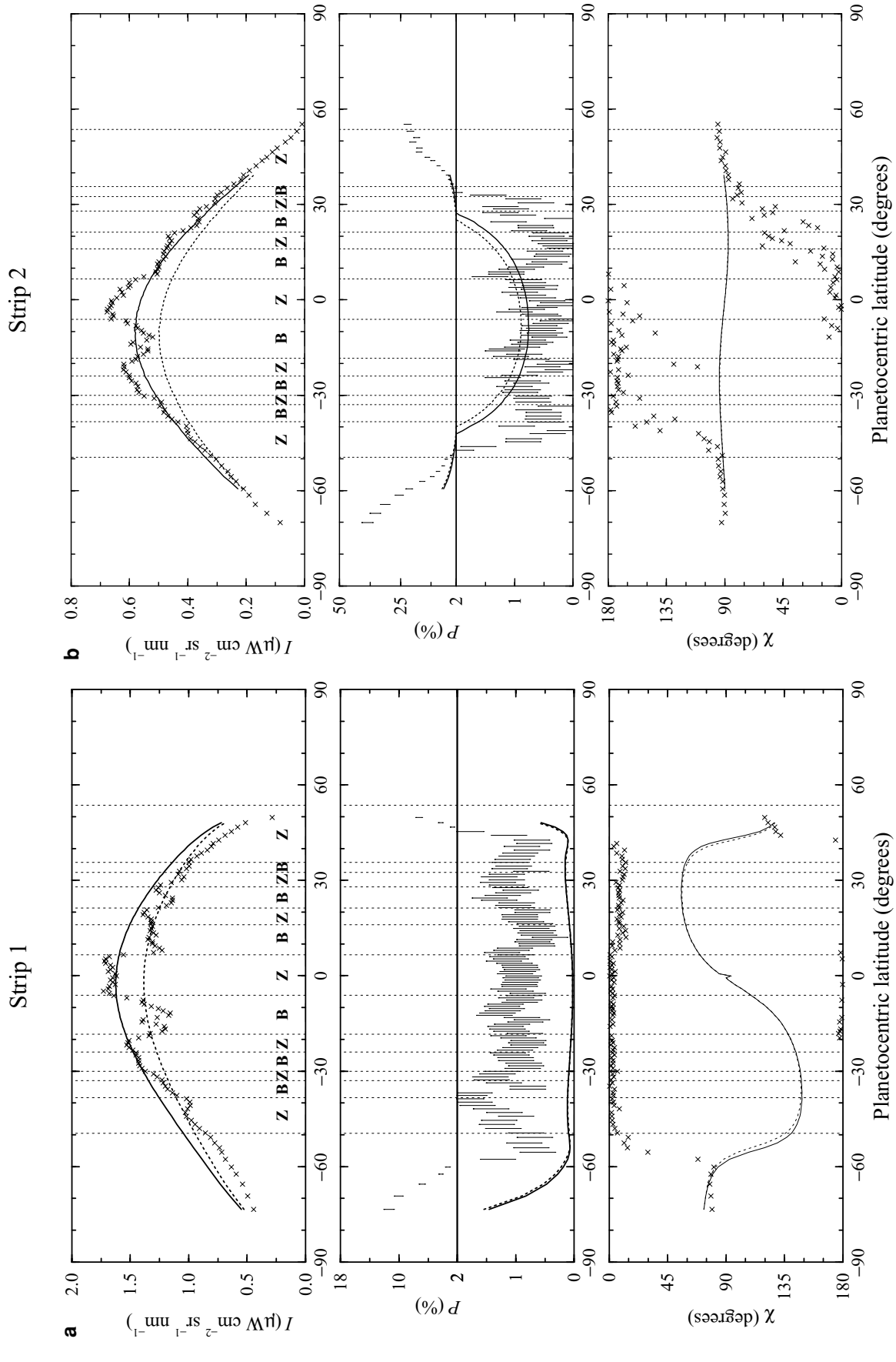

FIG. 4. Observed and calculated brightness (I), degree of linear polarization (P), and direction of polarization with respect to the scattering plane (χ) as functions of latitude for the four south–north strips. Each of the plots showing the degree of linear polarization is split into two parts with different scalings. Crosses and bars: observed values. Random errors of I are within the size of the symbols; no errors are known for χ. Solid curves: results of multiple-scattering calculations using the nominal models with $a_c = 0.997$ (STrZ model). Dashed curves: like solid, but with $a_c = 0.9925$ (SEBn model). The boundaries between belts (B) and zones (Z) are indicated by vertical dotted lines. Their latitudes are taken from the long-term averages given in Table 3.1 of Rogers (1995) and converted to planetocentric latitudes.

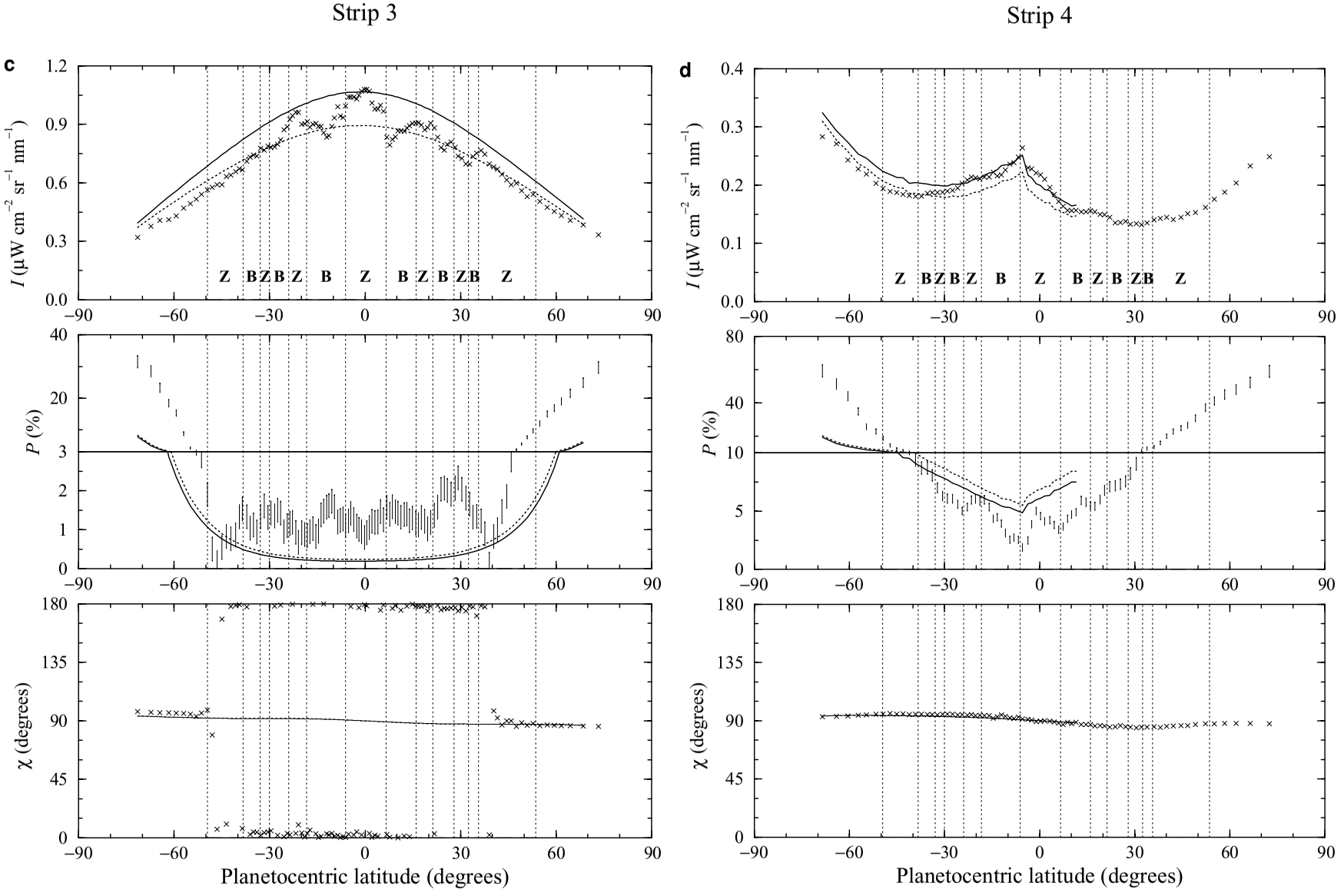

FIG. 4—*Continued*

The observed direction of polarization, χ_{obs}, exhibits a quasi-discrete nature: most values are clustered close to 0, 90, or 180°. Striking is the fact that for Strips 1, 2, and 3, χ_{obs} jumps from approximately 90° to approximately 0° or approximately 180° (note that these two values are equivalent) and back to approximately 90°, going from south to north. A plausible explanation is that at least one of the constituents of the jovian atmosphere at lower latitudes produces negative polarization. In the nominal models, the cloud particles do just that, but the calculated directions of polarization indicate that more negative polarization is required: only for Strip 1 does χ_{calc} deviate noticeably from 90° at some latitudes. For Strip 4, all pixels exhibit polarization nearly perpendicular to the local scattering plane. For that strip, the angle θ_0 is near grazing for all latitudes (notice in Fig. 1 that the strip runs close to the terminator) and the gas and haze particles produce such strong positive polarization (cf. Fig. 3 at a scattering angle of 81°) that the polarization of the atmosphere as a whole is perpendicular to the local scattering plane.

In general, no clear correlations between the brightness and the degree of linear polarization are evident. Particularly, belt/zone structures that are evident in the plots of the brightness (as mentioned above) are absent in the plots of the degree of linear polarization. It should be noted, however, that the brightness peak in the South Equatorial Belt at about −13° latitude in Strip 1 anticorrelates well with a dip in the degree of linear polarization. Strip 2 shows a similar peak in the brightness at this latitude but no corresponding feature in the degree of linear polarization.

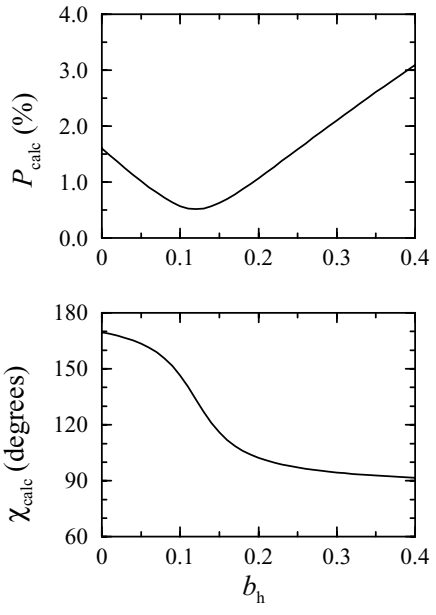

FIG. 5. Calculated degree of linear polarization, P_{calc}, and direction of polarization χ_{calc}, as functions of b_h for a pixel taken from Strip 2. Here, $p_c = -0.2$. For the other parameters, values were taken from Table III, with $a_c = 0.977$. For this pixel, $\mu = 0.844$, $\mu_0 = 0.424$, and $\phi - \phi_0 = 125°$.

5. QUANTITATIVE ANALYSIS

The latitudinal brightness variations and the increase of the degree of linear polarization toward the poles (see Fig. 4) both indicate that the atmosphere of Jupiter cannot be modeled by a single, horizontally homogeneous atmospheric model. As suggested in the preceding section, the single-scattering albedo of the cloud particles, a_c, and the haze optical thickness, b_h, are suitable candidates for atmospheric properties that vary across the disk. In this section, values for these parameters are derived from the observed brightness and degree of linear polarization on a pixel-wise basis.

5.1. Method of Analysis

For a pixel, values of a_c and b_h are sought in the (a_c, b_h)-parameter space that satisfy the following set of equations.

$$I_{calc}(a_c, b_h) - I_{obs} = 0, \tag{17}$$

$$P_{calc}(a_c, b_h) - P_{obs} = 0, \tag{18}$$

where I_{calc} and $P_{calc} = \sqrt{Q_{calc}^2 + U_{calc}^2}/I_{calc}$ are the calculated brightness and degree of linear polarization, respectively, for that pixel. Q_{calc} and U_{calc} are the calculated second and third Stokes parameters, respectively, for that pixel. The (a_c, b_h)-parameter space consists of all points (a_c, b_h) with $0 \le a_c \le 1$ and $b_h \ge 0$. For solving Eqs. (17) and (18), a Newton–Raphson algorithm was employed, using numerically calculated derivatives (Press *et al*. 1992) and initial values obtained from lookup tables as described below.

Equations (17) and (18) may yield zero, one, or more solutions. That there may be more than one solution can be explained as follows. In our calculations, it turned out that for any pixel, $I_{calc}(a_c, b_h)$ is a monotonic function of a_c, with b_h fixed, as well as of b_h, with a_c fixed. On the other hand, $P_{calc}(a_c, b_h)$ may not be monotonic in that sense for some pixels. This is illustrated in Fig. 5 for a typical pixel for which this occurs. For this illustration, we consider a certain fixed value for a_c, and let b_h increase, starting with $b_h = 0$. Then, χ_{calc} starts at a certain value, which is mainly determined by the cloud particles that produce negative polarization (notice that in Fig. 5, $\chi_{calc} \approx 180°$ for $b_h = 0$). Initially, P_{calc} decreases with increasing b_h due to the influence of the haze particles that produce positive polarization. Subsequently, P_{calc} increases for still higher values of b_h when the polarization of the haze particles dominates that of the cloud particles, so that $\chi_{calc} \approx 90°$. Thus, depending on the value of P_{obs}, more than one solution, with distinct values of χ, may be found for a pixel.

We consider a solution "acceptable" if the direction of polarization pertaining to that solution, χ_{calc}, deviates less than a tolerance β (say 20°) from the observed direction of polarization, χ_{obs}. Here, we have to take into account that $\chi = 0°$ is equivalent with $\chi = 180°$ even though the numerical values are 180° apart. Therefore, we distinguish three cases for χ_{obs} and

accept solutions

(i) for $\beta \leq \chi_{obs} \leq 180^\circ - \beta$ if

$$|\chi_{calc} - \chi_{obs}| < \beta, \tag{19}$$

(ii) for $\chi_{obs} < \beta$ if

$$\chi_{calc} - \chi_{obs} < \beta, \tag{20}$$

$$\text{or} \quad \chi_{calc} - \chi_{obs} > 180^\circ - \beta, \tag{21}$$

and (iii) for $\chi_{obs} > 180^\circ - \beta$ if

$$\chi_{obs} - \chi_{calc} < \beta, \tag{22}$$

$$\text{or} \quad \chi_{obs} - \chi_{calc} > 180^\circ - \beta. \tag{23}$$

Since for a pixel, more than one solution may exist, it is important that accurate initial values are put into the Newton–Raphson formalism. In order to find such values, lookup tables are produced for all combinations of a number of values for a_c and b_h. For b_h, the following values were chosen: $b_h = 0$ through 2.0 with steps of 0.05. Inspired by theoretical results of Sobolev (1975) (Sections 2.6 and 9.3) for semiinfite atmospheres, we considered a piecewise equidistant sequence for $\sqrt{1 - a_c}$ rather than for a_c, namely $\sqrt{1 - a_c} = 0$ through 0.20, with steps of 0.01. These values correspond to values of a_c ranging from 0.96 to 1. In this domain of a_c, the calculated brightnesses turned out to behave much more linearly as a function of $\sqrt{1 - a_c}$ than as a function of a_c. The above ranges for b_h and a_c were found to be sufficiently large. Nevertheless, we added $b_h = 20{,}000$ (this value is used as the numerical equivalent of infinity) and $\sqrt{1 - a_c} = 1.0$ ($a_c = 0$) in order to cover essentially the entire parameter space. Subsequently, linear interpolation is employed for fixed values of b_h to find the curve in the (a_c, b_h)-parameter space for which Eq. (17) holds (there is only one such curve due to the aforementioned monotonic behavior of $I_{calc}(a_c, b_h)$ both as a function of a_c and as a function of b_h). Then, linear interpolation along that curve is employed to search for solutions of Eq. (18). Note that because the interpolations are linear, certain solutions may be overlooked. However, tests performed with other sequences indicate that this does not affect our conclusions.

Endpoints for the error bars of the derived a_c and b_h are calculated by solving Eqs. (17) and (18) with $P_{obs} \pm \Delta P_{obs}$ as the second term on the left-hand side of Eq. (18). This approach generally results in asymmetric error bars since the left-hand sides of Eqs. (17) and (18) are nonlinear. If a solution for such an endpoint did not exist, we used the values for a_c and b_h that are on the edge of the (a_c, b_h)-parameter space and also on the curve through that space for which Eq. (17) holds. As mentioned above, the random errors of the brightness, ΔI_{obs}, are negligible (see Section 4). Of course, the systematic errors of the brightness, which may be quite large (see Section 2), do influence the derived values (especially those of a_c), but the behavior of the derived values as a function of latitude is hardly affected.

5.2. *Results Using the Nominal Models*

Shown in Fig. 6 are the results of an analysis for which we used the values listed in Table III for the fixed parameters and $\beta = 20^\circ$ for the acceptance criterion expressed in Eqs. (19)–(23). Acceptable solutions are shown as solid circles, unacceptable solutions as open circles. As in Section 4, only pixels with $\mu > 0.15$ and $\mu_0 > 0.15$ were considered.

For Strip 1, hardly any acceptable solution is found. At midlatitudes, the observed degree of linear polarization was reproduced, but in those cases, the calculated direction of polarization was incompatible with the observed values. For many pixels at higher and lower latitudes, even such a limited agreement turned out not to be possible (notice that the solid and dashed curves in Fig. 4 extend to higher latitudes than the results in Fig. 6). For these pixels, the haze optical thickness would have to assume such high values in order to reproduce the observed degree of linear polarization that even for a cloud single-scattering albedo of 1, the calculated brightness would be lower than the observed brightness.

The results for Strips 2, 3, and 4 agree better with the qualitative inferences described in Section 4. That is, the haze optical thickness is low at equatorial and midlatitudes and increases steeply towards higher latitudes, while the behavior of the single-scattering albedo of the cloud particles follows that of the observed brightness. However, note that for Strips 2 and 3, as for Strip 1, hardly any solution at equatorial and midlatitudes is acceptable. Particularly, the nominal models fail to yield satisfactory results for these strips at the latitudes of the STrZ and the SEBn. A possible explanation for this is changes in the atmosphere since the Pioneer observations in 1973 and 1974.

5.3. *Results for Adjusted Models*

If we assume that the direction of polarization of the reflected sunlight is mostly determined by single scattering, a plausible adjustment to find acceptable solutions at equatorial and midlatitudes is to decrease the value of p_c. A value of $p_c = -0.20$ instead of -0.05 indeed relieves the problem for Strips 2 and 3. But for Strip 1, with a typical local phase angle of 14°, even a scattering matrix with a value of $p_c = -1$ does not yield satisfactory results. Note here that, apart from the fact that such a scattering matrix is unrealistic, the signed degree of linear polarization, P_s, equals only -3% for such a scattering matrix at a scattering angle of 166° (180° minus the typical local phase angle of Strip 1) for single scattering when the incident light is unpolarized.

Yet, for certain collections of particles, it may occur that at large scattering angles, the function $-F_{21}(\Theta)/F_{11}(\Theta)$ decreases with increasing scattering angle and then assumes values smaller than -3%. This is, for instance, the case in results of laboratory measurements of ammonia ice crystals (one of the prime candidates for the constituents of Jupiter's cloud layer) (Pope *et al.* 1992; see also Section 5.4). Since such a decrease

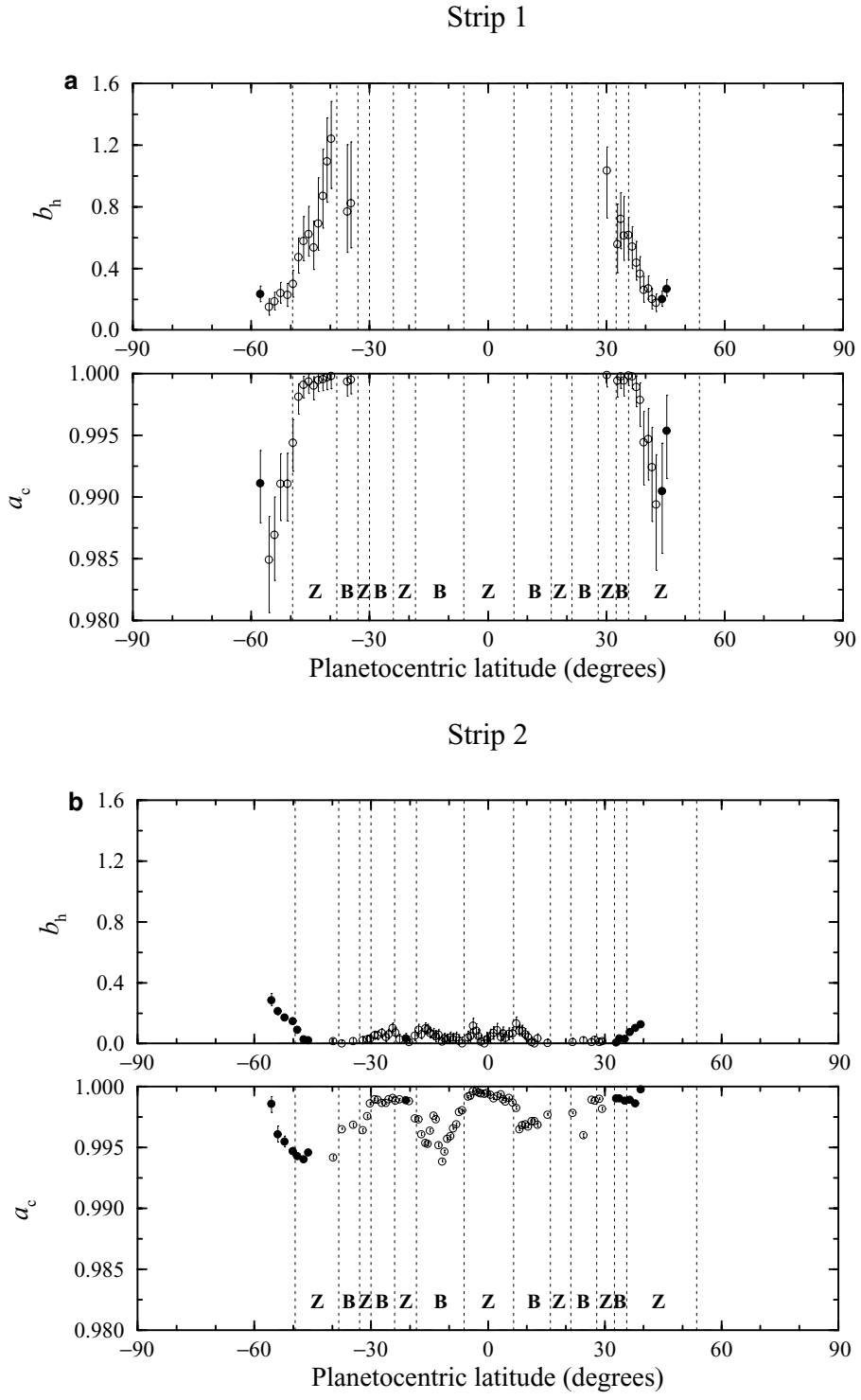

FIG. 6. Derived values and error bars for the haze optical thickness and single-scattering albedo of the cloud particles for the four south–north strips using the nominal parameter values listed in Table III for the fixed parameters. Filled circles indicate solutions with acceptable values of the calculated direction of polarization. Open circles indicate unacceptable solutions. Belt/zone boundaries are indicated by vertical dotted lines (see Fig. 4).

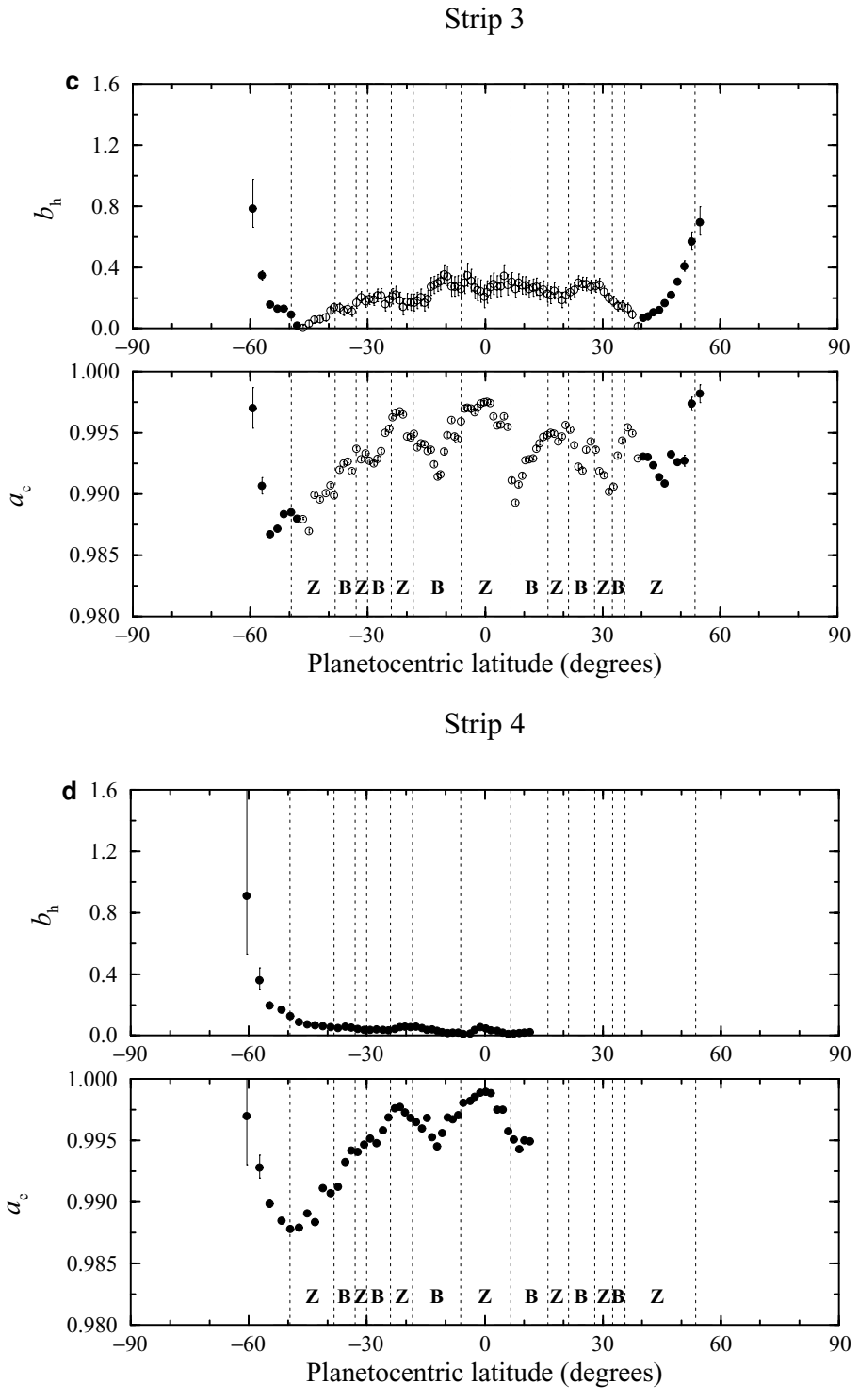

FIG. 6—*Continued*

does not occur in our present parameterization (Eq. (9)) if $p < 0$, an adjustment of Eq. (9) was necessary. Subsequently, we tested whether such an adjustment increased the number of acceptable solutions for the strips considered, in particular for Strip 1. The adjustment we implemented involved adding a term to Eq. (9), yielding

$$-\frac{F_{21}(\Theta)}{F_{11}(\Theta)} = p_c \frac{1-\cos^2\Theta}{1+\cos^2\Theta} + q_c \frac{1-\nu(\cos\Theta)^2}{1+\nu(\cos\Theta)^2}, \qquad (24)$$

where $-1 \le p_c \le 1$, $-1 \le q_c \le 1$, $0^\circ < \Theta_0 < 180^\circ$, and $\nu(\cos\theta)$ is a function of $\cos\Theta$ such that $\nu = -1$, 0, and 1 if $\cos\Theta = -1$, $\cos\Theta_0$, and 1, respectively. This makes the shape of the added term as a function of scattering angle similar to that of the first term, but it has its extremum at a $\Theta = \Theta_0$ rather than at $\Theta = 90^\circ$. We used the rational function

$$\nu(\cos\Theta) = \frac{\cos\Theta - \cos\Theta_0}{1 - \cos\Theta_0 \cos\Theta}. \quad (25)$$

Generally, scattering matrices with their 2,1-elements defined by Eq. (24) and the other elements defined as in Section 3 do not obey the Cloude coherency matrix test (cf. Hovenier and Van der Mee 1996, Braak *et al*. 2001). Therefore, we also adjusted Eq. (11), yielding

$$\frac{F_{33}(\Theta)}{F_{11}(\Theta)} = \frac{1}{|p_c| + |q_c|}\left(|p_c|\frac{2\cos\Theta}{1+\cos^2\Theta} + |q_c|\frac{2\nu}{1+\nu^2}\right). \quad (26)$$

With this parameterization, the Cloude coherency matrix test is fulfilled at least as long as $|p_c| + |q_c| \le 1$, while necessary requirements at 0 and 180° scattering angles are obeyed as well (cf. Hovenier and Van der Mee 1996, Braak *et al*. 2001). Thus all constraints are taken into account.

We replaced the scattering matrix of the cloud particles employed so far by a parameterized scattering matrix using Eqs. (24) and (26) with $p_c = -0.2$, $\Theta_0 = 166^\circ$, and $q_c = -0.1$. The functions $F_{11}(\Theta)$ and $-F_{21}(\Theta)/F_{11}(\Theta)$ of this adjusted scattering matrix are shown in Fig. 7, compared with the corresponding functions of the nominal models and with results of laboratory measurements reported by Pope *et al*. (1992).

In Fig. 8, derived values of the haze optical thickness and the single-scattering albedo of the cloud particles using this adjusted scattering matrix are shown. In comparison with Fig. 6, acceptable solutions were found for many more pixels, especially throughout the equatorial and midlatitudes. Many pixels on Strips 2 and 3 yielded even two solutions, only one of which is acceptable. With the adjusted parameterized scattering matrix, the observations at the highest latitudes could still not be reproduced without varying at least one of the parameters that was fixed in the above analysis. We found that by increasing the haze single-scattering albedo, a_h, or decreasing the asymmetry parameter of the haze particles, g_h, it was possible to find solutions extending to higher latitudes.

The results shown in Fig. 8 may be summarized as follows. The derived values of the haze optical thickness at equatorial and midlatitudes are generally on the order of about a tenth, except for Strip 1. Toward the poles, b_h rises steeply to several tenths. On smaller spatial scales, the derived haze optical thickness shows the same small-scale features as the observed degree of linear polarization. For Strip 1, derived values of b_h are somewhat larger than for the other strips and show more variation with latitude.

The derived single-scattering albedo of the cloud particles is determined mainly by (and shows the same small-scale features as) the observed brightness throughout the latitude ranges of all four south–north strips. Therefore, the belt–zone structure is apparent for all four strips. That the derived values of a_c differ so much between different strips may be caused by imperfections in the phase functions that were employed in the analysis (which were one- or two-term Henyey–Greenstein functions).

As was the case for the observed brightnesses and degrees of linear polarization, no clear correlations were found between the derived single-scattering albedos of the cloud particles and the derived haze optical thicknesses.

5.4. *Discussion*

It is not surprising that our analysis shows that at least one of the constituents of the jovian atmosphere produces negative polarization at large scattering angles, since results of Morozhenko and Yanovitskii (1973) already indicated this. Besides, negative

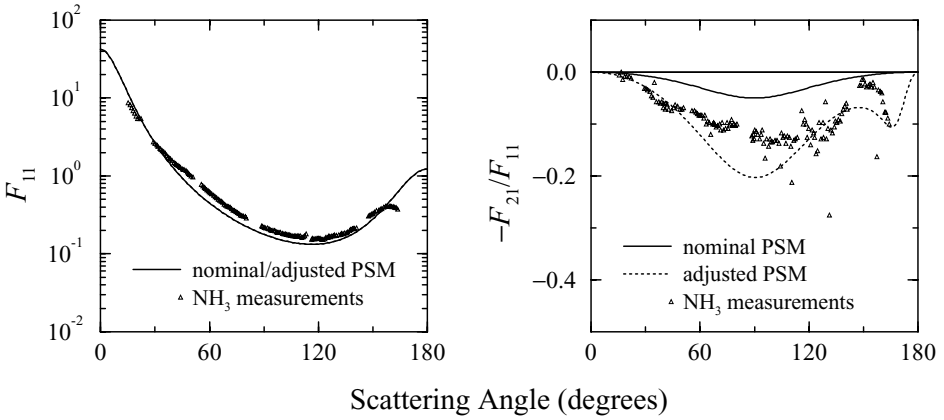

FIG. 7. The functions $F_{11}(\Theta)$ and $-F_{21}(\Theta)/F_{11}(\Theta)$ of the scattering matrix of the cloud particles in the nominal models (identical to the dashed curves in Fig. 3) and of the adjusted parameterized scattering matrix with $p_c = -0.2$, $\Theta_0 = 166^\circ$, and $q_c = -0.1$ in Eqs. (24) and (26). "PSM" stands for parameterized scattering matrix. The triangles represent laboratory measurements at 652 nm of ammonia ice crystals grown at a temperature of 180 K as reported by Pope *et al*. (1992).

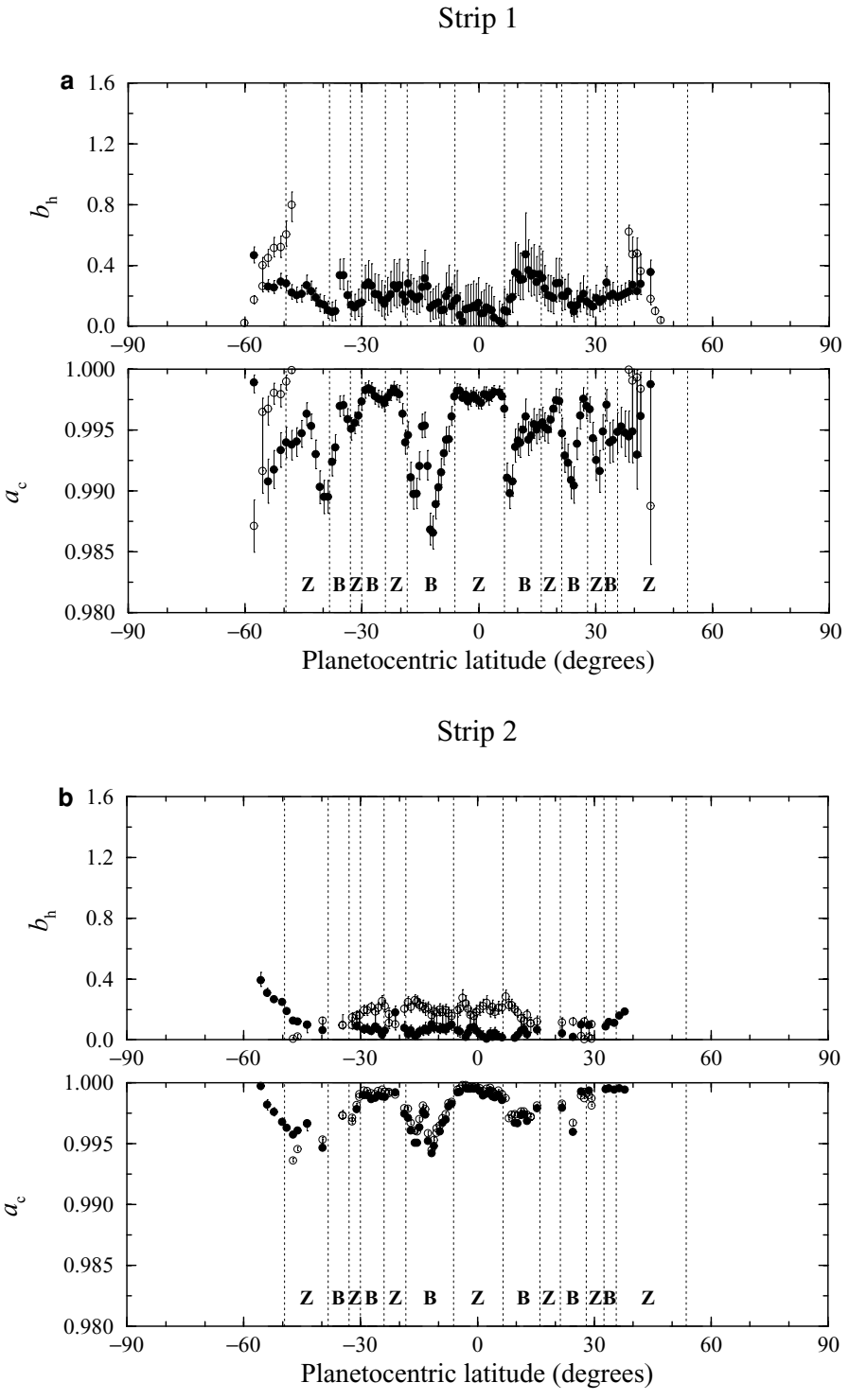

FIG. 8. Same as Fig. 6 but with the scattering matrix of the cloud particles replaced by the adjusted parameterized scattering matrix.

polarization at large scattering angles for visible wavelengths has been observed for many particles in the Solar System, such as dust particles—e.g., zodiacal light, planetary regoliths, and cometary comas (cf. Lumme 2000)—and the cloud particles of Venus (Hansen and Hovenier 1974) and Saturn (Tomasko and Doose 1984). The particles of the jovian and venusian clouds produce negative polarization not only at large scattering angles but also for side scattering. This differs from the other particles mentioned, since these exhibit positive polarization for side scattering. That Smith and Tomasko (1984) did not find such

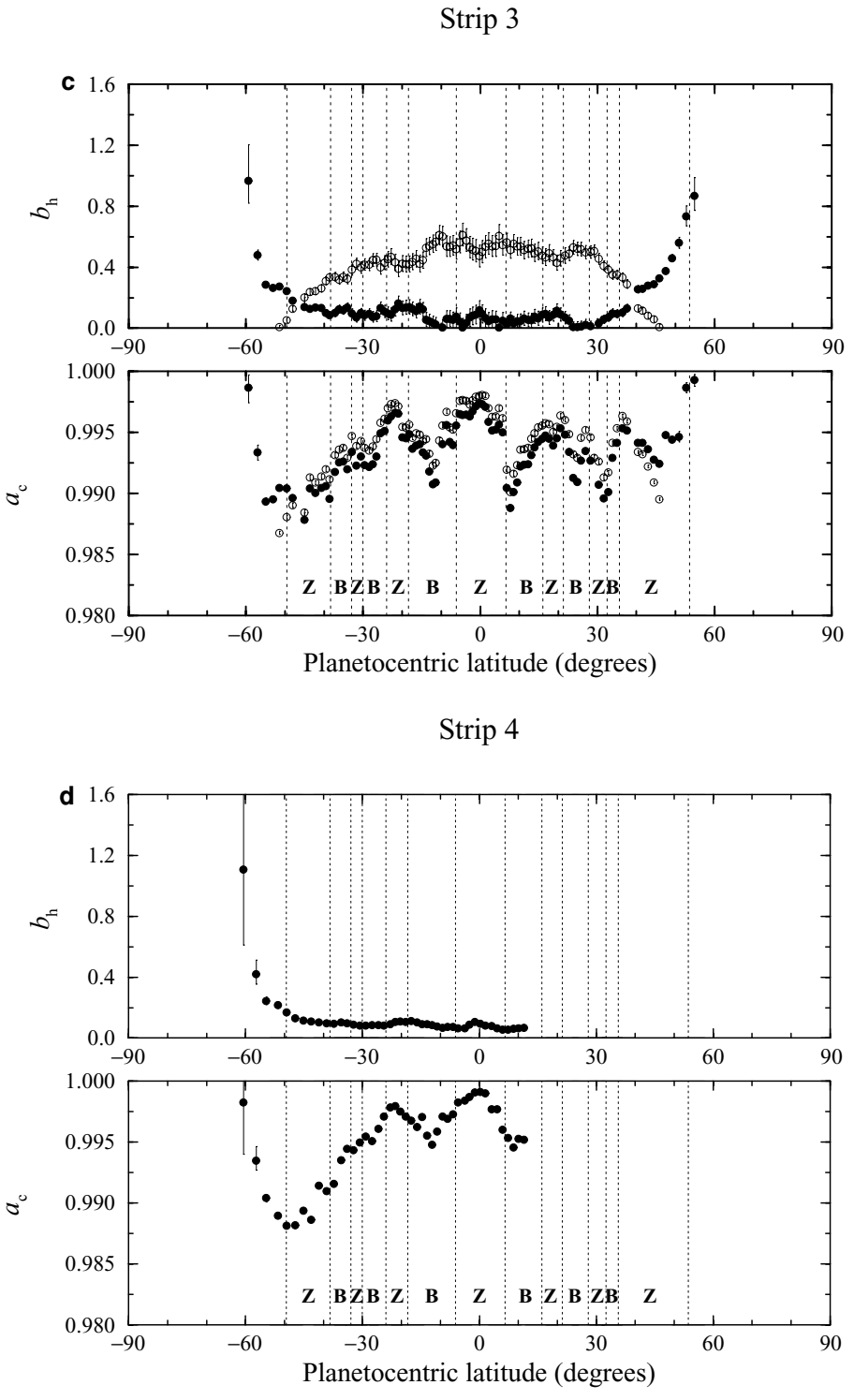

FIG. 8—*Continued*

strong negative polarization at large scattering angles for the jovian cloud particles may be caused by the fact that they did not use polarization measurements obtained at phase angles smaller than 43°.

The temperature and pressure at which particles form affect the sizes and shapes of these particles, and hence their single-scattering properties. Therefore, the shapes of the derived $F_{11}(\Theta)$ and $-F_{21}(\Theta)/F_{11}(\Theta)$ as functions of Θ may give an indication

of the temperature and pressure under which cloud particles form and grow in the upper part of Jupiter's cloud layer. In that respect, it is interesting to compare our results with those of Pope *et al*. (1992). In that study, ammonia crystals were grown in the laboratory at various temperatures. Their results obtained at a temperature of 180 K (see also Fig. 7) fit our adjusted scattering matrix best. Additional laboratory measurements (e.g., at various pressures) are required for making solid inferences.

6. CONCLUDING REMARKS

During the nominal mission of the Galileo Orbiter, the photopolarimeter/radiometer on board that spacecraft performed several brightness and polarization observations of Jupiter. In this paper, we studied the four south–north strips of measurements of the brightness, the degree of linear polarization, and the direction of polarization at 678.5 nm. For a quantitative analysis of the data, we employed an atmospheric model that includes a haze layer above a cloud layer. In order to keep the number of model parameters small and because the shapes of the haze and cloud particles are unknown, we employed parameterized scattering matrices for those particles obeying all constraints. Nominal models were chosen that are virtually the same as models derived by Smith and Tomasko (1984) for the South Tropical Zone and the north component of the South Equatorial Belt. Values of two designated free parameters were derived on a pixel-wise basis from the measured brightness and degree of linear polarization.

The measured direction of polarization was used to determine if a pair of values that sufficiently reproduced the measured brightness and degree of linear polarization was acceptable. Our study shows that for purposes such as these, it is very important that the direction of polarization be measured as accurately as possible, as well as the orientation of the reference plane with respect to which this direction of polarization is measured.

The main results of our analyses, which are described in Sections 5.3 and 5.4, could not be obtained unless we adjusted the function $-F_{21}(\Theta)/F_{11}(\Theta)$ of the cloud particles derived by Smith and Tomasko (1984). In this paper, we provided an ad-hoc parameterization (Eqs. (24)–(26)) that implemented this adjustment. More results of laboratory measurements as well as theoretical single-scattering calculations are necessary both for the further development of realistic parameterizations of scattering matrices and for the interpretation of values of the parameters of such parameterized scattering matrices that are derived from brightness and polarization measurements.

The measurements considered in this paper constitute about 6% of all brightness and polarization measurements of Jupiter obtained by the PPR during Galileo's nominal mission and pertain to only a few parts of the entire phase angle range $0^\circ \leq \alpha \leq 180^\circ$. By demanding that results at different phase angles be consistent and analyzing the remainder of the data, more accurate determinations of single-scattering properties of jovian atmospheric constituents should be possible.

ACKNOWLEDGMENTS

It is a pleasure to express our gratitude to Glenn Orton, Bob West, Peter Gierasch, and John McAnally for fruitful discussions and correspondence. This work has been supported in part by a Columbia University research program funded by NASA Goddard Institute for Space Studies.

REFERENCES

Braak, C. J., J. F. De Haan, C. V. M. Van der Mee, J. W. Hovenier, and L. D. Travis 2001. Parameterized scattering matrices for small particles in planetary atmospheres. *J. Quant. Spectrosc. Radiat. Transfer* **69**, 585–604.

Braak, C. J., J. F. De Haan, J. W. Hovenier, and L. D. Travis 2002. Spatial and temporal variations of Venus haze properties obtained from Pioneer Venus Orbiter polarimetry. *J. Geophys. Res*., in press.

Carlson, B. E., and B. L. Lutz 1989. Spatial and temporal variations in the atmosphere of Jupiter: Polarimetric and photometric constraints. In *Time-Variable Phenomena in the Jovian System* (M. J. S. Belton, R. A. West, and J. Rahe, Eds.), pp. 289–296. Natl. Aeronautics & Space Admin., Washington, DC.

Chandrasekhar, S. 1950. *Radiative Transfer*. Oxford Univ. Press, London/Dover, New York, 1960.

Coffeen, D. L. 1974. Optical polarization measurements of the Jupiter atmosphere at 103° phase angle. *J. Geophys. Res*. **79**, 3645–3652.

De Haan, J. F., P. B. Bosma, and J. W. Hovenier 1987. The adding method for multiple scattering calculations of polarized light. *Astron. Astrophys*. **183**, 371–391.

Dollfus, A. 1957. Étude des planètes par la polarisation de leur lumière. *Suppl. Ann. Astrophys*. **4**, English trans.: NASA TT F-188, 1964.

Dollfus, A. 1990. Une nouvelle méthode d'analyse polarimétrique des surfaces planétaires. *Comptes Rendues Acad. Sci. Paris* **311**, 1185–1190.

Gehrels, T., B. H. Herman, and T. Owen 1969. Wavelength dependence of polarization. XIV. Atmosphere of Jupiter. *Astron. J*. **74**, 190–199.

Hall, J. S., and L. A. Riley 1968. Photoelectric observations of Mars and Jupiter with a scanning polarimeter. *Lowell Obs. Bull*. **7**, 83–92.

Hall, J. S., and L. A. Riley 1969. Polarization measures of Jupiter and Saturn. *J. Atmos. Sci*. **26**, 920–923.

Hall, J. S., and L. A. Riley 1974. Polarization measurements of Jupiter and the Great Red Spot. In *Planets, Stars and Nebulae Studied with Photopolarimetry* (T. Gehrels, Ed.), pp. 593–598. Univ. of Arizona Press, Tucson.

Hansen, J. E. 1971. Multiple scattering of polarized light in planetary atmospheres. Part I. The doubling method. *J. Atmos. Sci*. **28**, 120–125.

Hansen, J. E., and J. W. Hovenier 1971. The doubling method applied to multiple scattering of polarized light. *J. Quant. Spectrosc. Radiat. Transfer* **11**, 809–812.

Hansen, J. E., and J. W. Hovenier 1974. Interpretation of the polarization of Venus. *J. Atmos. Sci*. **31**, 1137–1160.

Henyey, L. G., and J. L. Greenstein 1941. Diffuse radiation in the galaxy. *Astrophys. J*. **93**, 70–83.

Horak, H. G. 1950. Diffuse reflection by planetary atmospheres. *Astrophys. J*. **112**, 445–463.

Hovenier, J. W. 1970. Principles of symmetry for polarization studies of planets. *Astron. Astrophys*. **7**, 86–90.

Hovenier, J. W. 1971. Multiple scattering of polarized light in planetary atmospheres. *Astron. Astrophys*. **13**, 7–29.

Hovenier, J. W., and C. V. M. Van der Mee 1983. Fundamental relationships relevant to the transfer of polarized light in a scattering atmosphere. *Astron. Astrophys*. **128**, 1–16.

Hovenier, J. W., and C. V. M. Van der Mee 1996. Testing scattering matrices: A compendium of recipes. *J. Quant. Spectrosc. Radiat. Transfer* **55**, 649–661.

Kawabata, K., D. L. Coffeen, J. E. Hansen, W. A. Lane, M. Sato, and L. D. Travis 1980. Cloud and haze properties from Pioneer Venus polarimetry. *J. Geophys. Res.* **85**, 8129–8140.

Kemp, J. C. 1974. Circular polarization of planets. In *Planets, Stars and Nebulae Studied with Photopolarimetry* (T. Gehrels, Ed.), pp. 607–616. Univ. of Arizona Press, Tucson.

Knibbe, W. J. J., J. F. De Haan, J. W. Hovenier, and L. D. Travis 1997. A biwavelength analysis of Pioneer Venus polarization observations. *J. Geophys. Res.* **102**, 10,945–10,957.

Knibbe, W. J. J., J. F. De Haan, J. W. Hovenier, and L. D. Travis 1998. Analysis of temporal variations of the polarization of Venus observed by Pioneer Venus Orbiter. *J. Geophys. Res.* **103**, 8557–8574.

Lumme, K. 2000. Scattering properties of interplanetary dust particles. In *Light Scattering by Nonspherical Particles: Theory, Measurements, and Applications* (M. I. Mishchenko, J. W. Hovenier, and L. D. Travis, Eds.), pp. 555–583. Academic Press, San Diego.

Lyot, B. 1929. Recherches sur la polarisation de la lumière des planètes et de quelques substances terrestres. *Ann. Obs. Paris (Meudon)* **8**, English trans.: NASA TT F-187, 1964.

Mishchenko, M. I. 1990. Physical properties of the upper tropospheric aerosols in the equatorial region of Jupiter. *Icarus* **84**, 296–304.

Mishchenko, M. I., and L. D. Travis 1997a. Satellite retrieval of aerosol properties over the ocean using measurements of reflected sunlight: Effect of instrumental errors and aerosol absorption. *J. Geophys. Res.* **102**, 13,543–13,553.

Mishchenko, M. I., and L. D. Travis 1997b. Satellite retrieval of aerosol properties over the ocean using polarization as well as intensity of reflected sunlight. *J. Geophys. Res.* **102**, 16,989–17,013.

Morozhenko, A. V., and E. G. Yanovitskii 1973. The optical properties of Venus and the jovian planets. I. The atmosphere of Jupiter according to polarimetric observations. *Icarus* **18**, 583–592.

Neckel, H., and D. Labs 1984. The solar radiation between 3300 and 12500 Å. *Solar Phys.* **90**, 205–258.

Pope, S. K., M. G. Tomasko, M. S. Williams, M. L. Perry, L. R. Doose, and P. H. Smith 1992. Clouds of ammonia ice: Laboratory measurements of the single-scattering properties. *Icarus* **100**, 203–220.

Press, W. H., S. A. Teukolsky, W. T. Vetterling, and B. P. Flannery 1992. *Numerical Recipes: The Art of Scientific Computing,* 2nd ed. Cambridge Univ. Press, New York.

Pryor, W. R., and C. W. Hord 1991. A study of photopolarimeter system UV absorption data on Jupiter, Saturn, Uranus, and Neptune: Implications for auroral haze formation. *Icarus* **91**, 161–172.

Rages, K., R. Beebe, and D. Senske 1999. Jovian stratospheric hazes: The high phase angle view from Galileo. *Icarus* **139**, 211–226.

Rogers, J. H. 1995. *The Giant Planet Jupiter*. Cambridge Univ. Press, Cambridge. UK.

Russell, E. E., F. G. Brown, R. A. Chandos, W. C. Fincher, L. F. Kubel, A. A. Lacis, and L. D. Travis 1992. Galileo photopolarimeter/radiometer experiment. *Space Sci. Rev.* **60**, 531–563.

Sato, M., L. D. Travis, and K. Kawabata 1996. Photopolarimetry analysis of the Venus atmosphere in polar regions. *Icarus* **124**, 569–585.

Smith, P. H. 1986. The vertical structure of the jovian atmosphere. *Icarus* **65**, 264–279.

Smith, P. H., and M. G. Tomasko 1984. Photometry and polarimetry of Jupiter at large phase angles. II. Polarimetry of the South Tropical Zone, South Equatorial Belt, and the polar regions from the Pioneer 10 and 11 missions. *Icarus* **58**, 35–73.

Sobolev, V. V. 1975. *Light Scattering in Planetary Atmospheres*. Pergamon, Oxford (original Russian 1972).

Tomasko, M. G., and L. R. Doose 1984. Polarimetry and photometry of Saturn from Pioneer 11: Observations and constraints on the distribution and properties of cloud and aerosol particles. *Icarus* **58**, 1–34.

Tomasko, M. G., and P. H. Smith 1982. Photometry and polarimetry of Titan: Pioneer 11 observations and their implications for aerosol properties. *Icarus* **51**, 65–95.

U. S. Government Printing Office 1997. *Astronomical Almanac*. U. S. Government Printing Office, Washington, DC.

Van de Hulst, H. C. 1957. *Light Scattering by Small Particles*. Wiley, New York/Dover, New York, 1981.

Van de Hulst, H. C. 1980. *Multiple Light Scattering: Tables, Formulas, and Applications*. Academic Press, New York.

Weidenschilling, S. J., and J. S. Lewis 1973. Atmospheric and cloud structures of the jovian planets. *Icarus* **20**, 465–476.

West, R. A. 1979. Spatially resolved methane band photometry of Jupiter. I. Absolute reflectivity and center-to-limb variations in the 6190-, 7250-, and 8900-Å bands. *Icarus* **38**, 12–33.

West, R. A., and P. H. Smith 1991. Evidence for aggregate particles in the atmospheres of Titan and Jupiter. *Icarus* **90**, 330–333.

West, R. A., C. W. Hord, K. E. Simmons, D. L. Coffeen, M. Sato, and A. L. Lane 1981. Near-ultraviolet scattering properties of Jupiter. *J. Geophys. Res.* **86**, 8783–8792.

West, R. A., D. F. Strobel, and M. G. Tomasko 1986. Clouds, aerosols, and photochemistry in the jovian atmosphere. *Icarus* **65**, 161–217.